23266879

SUBRETINAL DRUSENOID DEPOSITS IN NON-NEOVASCULAR AGE-RELATED MACULAR DEGENERATION

Morphology, Prevalence, Topography, and Biogenesis Model

CHRISTINE A. CURCIO, PHD,* JEFFREY D. MESSINGER, DC,* KENNETH R. SLOAN, PHD,† GERALD MCGWIN, PHD, MS,‡ NANCY E. MEDEIROS, MD,§ RICHARD F. SPAIDE, MD¶

Purpose: To characterize the morphology, prevalence, and topography of subretinal drusenoid deposits, a candidate histological correlate of reticular pseudodrusen, with reference to basal linear deposit (BlinD), a specific lesion of age-related macular degeneration, and to propose a biogenesis model for both lesion.

Methods: Donor eyes with median death-to-preservation of 2:40 hours were postfixed in osmium tannic acid paraphenylenediamine and prepared for macula-wide high-resolution digital sections. Annotated thicknesses of 21 chorioretinal layers were determined at standard locations in sections through the fovea and the superior perifovea.

Results: In 22 eyes of 20 white donors (83.1 ± 7.7 years), SDD appeared as isolated or confluent drusenoid dollops punctuated by tufts of retinal pigment epithelium apical processes and associated with photoreceptor perturbation. Subretinal drusenoid deposits and BlinD were detected in 85 and 90% of non-neovascular age-related macular degeneration donors, respectively. Subretinal drusenoid deposit was thick (median, 9.4 μm) and more abundant in the perifovea than in the fovea ($P < 0.0001$). BlinD was thin (median, 2.1 μm) and more abundant in the fovea than in the perifovea ($P < 0.0001$).

Conclusion: Subretinal drusenoid deposits and BlinD prevalence in age-related macular degeneration eyes are high. Subretinal drusenoid deposits organized morphology, topography, and impact on surrounding photoreceptors imply specific processes of biogenesis. Contrasting topographies of subretinal drusenoid deposits and BlinD suggest relationships with differentiable aspects of rod and cone physiology, respectively. A 2-lesion 2-compartment biogenesis model incorporating outer retinal lipid homeostasis is presented.

RETINA 0:1–12, 2012

A lesion recently recognized in eyes with age-related macular degeneration (AMD) is subretinal drusenoid deposit (SDD).[1] Clinicopathologic studies by Sarks et al showed that membranous debris, the principal component of soft drusen and basal linear deposit (BlinD), is also found in vacuoles within the retinal pigment epithelium (RPE), basal mounds within basal laminar deposit (BlamD), and within the subretinal space.[2,3] The subretinal material was named SDD by one of the author (C.A.C.). Subretinal drusenoid deposit shares with soft drusen superficial ultrastructural and compositional similarities, including membrane-bounded particles with neutral lipid interiors, unesterified cholesterol (UC), apolipoprotein E (apoE), complement factor H, and vitronectin.[2–6] Conversely, SDD lacks immunoreactivity for photoreceptor, Müller cell, and RPE marker proteins. Subretinal drusenoid deposit of lateral length, 12 μm to 190 μm, was present in 9 and 22% of 2 small series of non-neovascular AMD eyes, respectively.[4,7] Because eyes in these histological studies were non-exhaustively sectioned, SDD width and prevalence may have been underestimated.

Subretinal drusenoid deposit has been linked to the phenotype reticular pseudodrusen, a lesion variably named and described, depending on the imaging modality, patient population, and investigators. First shown in blue light reflectance photography,[8] pseudodrusen

visible in the blue channel of color fundus photographs, and in near-infrared reflectance images were attributed to SDD in our previous studies, which revealed discrete collections of hyperreflective material in the subretinal space by spectral domain optical coherence tomography.[1,9] In an early direct clinicopathologic correlation, Sarks attributed reticular pseudodrusen seen in red-free photography or infrared reflectance to choroidal fibrosis in an AMD specimen lacking neurosensory retina.[10] They later changed this attribution to SDD after reviewing another specimen with an attached retina.[11]

More information about the histopathology of SDD would facilitate understanding of its role in AMD pathophysiology, including its relationship with AMD's signature sub-RPE lesion. Here, we report SDD morphology, prevalence, and topography in donor eyes meeting histopathologic criteria for non-neovascular AMD. To provide insight into SDD pathogenesis, we compared it with BlinD, a specific accumulation of material under the RPE in AMD that also forms mounds seen clinically as soft drusen.[2,12] We analyzed lesion morphology in systematically sampled high-resolution histological cross-sections of whole macula.[13] We found that SDD is robust and as prevalent as BlinD and located preferentially in the perifovea, in contrast to BlinD's predilection for the fovea. These distinct lesion topographies plausibly reflect differential aspects of rod and cone photoreceptor physiology.

Methods

This study used donor eyes accessioned for research from the Alabama Eye Bank (1995–2008). Median death-to-preservation time was 2:40 hours. Eyes were preserved by immersion in 1% paraformaldehyde and 2.5% glutaraldehyde in 0.1 M phosphate buffer after anterior segment removal. Donor eyes with gross macular appearance consistent with early AMD and unremarkable maculas from age-matched donors were sectioned and evaluated (n = 64 total). Maculas with retina in place and vitreous removed were subjected to ex vivo color photography with a dissection scope.[14] Tissue was postfixed by osmium tannic acid paraphenylenediamine for neutral lipids in extracellular AMD-associated lesion.[15,16] Macula-wide high-resolution sections were collected starting at the superior edge of an 8-mm diameter full-thickness punch[13,17] and stained with toluidine blue (Figure 1). Study sections were 2 mm superior in the foveal center, that is, within superior perifovea, where reticular pseudodrusen are abundant clinically, and in the foveola.

Clinical records were available for some donors but not all. Age-related macular degeneration case ascertainment used histopathologic criteria.[14,18] Criteria for non-neovascular AMD were a foveolar section lacking evidence of choroidal neovascularization or a fibrovascular scar AND either a druse >125 μm OR a severe RPE change (hyperplasia, multiple layers, anterior migration) AND either drusen OR continuous basal laminar deposit (BlamD).[3,14,19]

The use of digital sections scaled to tissue units (in micrometer), a fovea-centered coordinate system, and systematic sampling enabled comparisons of morphologic data across eyes and inference about the extent of macula affected by lesion. Sections were scanned with a 40× numerical aperture 0.95 objective, a robotic microscope stage, and image-stitching software (CellSens; Olympus, Center Valley, PA). Digital sections (~500 MB) were used for recording annotated thicknesses of chorioretinal layers.[13] Using custom plug-ins written for ImageJ (http://rsbweb.nih.gov/ij/), a single experienced observer (C.A.C.) sampled maculas at 25 locations from 3 mm nasal to 3 mm temporal. Thirteen locations were $\leq$1 mm of the foveal center where neurosensory retina cell density gradients change rapidly.[20,21] At each location, layer thicknesses were measured using the Segmented Lengths tool and layer-appropriate annotations chosen from a menu. Retinal pigment epithelium morphology and pigmentation was graded on an 8-point scale adapted from Vogt et al and Rudolf et al.[22,23] Glass slides were viewed with a 60× oil-immersion objective (numerical aperture = 1.4) in parallel with digital sections to inform judgments about small structures. Thicknesses and annotations were extracted by custom ImageJ plug-ins for analysis with spreadsheets (Excel 2008; Microsoft, Redmond, WA) and statistical software (StatPlus for Mac; SAS, Cary NC). Thicknesses accumulated relative to the RPE basal lamina were displayed as layer plots (Figure 2).

Thicknesses are reported for the subretinal space, RPE, BlamD, sub-RPE space, and choriocapillaris. In this postmortem material, neurosensory retina was detached at 72.7% of SDD-containing locations. Detachment may be accompanied by compaction of RPE apical processes into a layer of relatively uniform thickness. Alternatively, RPE apical processes may be

From the Departments of *Ophthalmology, †Computer and Information Science, and ‡Epidemiology, University of Alabama at Birmingham, Birmingham, Alabama; §Retina Specialists of North Alabama, Huntsville, Alabama; and ¶Vitreous Retina Macula Consultants of New York, New York, New York.

Supported by NIH grants EY06109, International Retinal Research Foundation, Research to Prevent Blindness, Inc, EyeSight Foundation of Alabama.

None of the authors have any conflicting interests to disclose.

Reprint requests: Christine A. Curcio, PhD, Department of Ophthalmology, EyeSight Foundation of Alabama Vision Research Laboratories, University of Alabama School of Medicine, 1670 University Boulevard Room 360, Birmingham, AL 35294-0099; e-mail: curcio@uab.edu

COLOR

Fig. 1. Macula-wide high-resolution section of an eye with non-neovascular AMD. A 0.8-μm-thick section of epoxy resin–embedded retina, choroid, and sclera; postfixed with osmium tannic acid paraphenylenediamine and stained with toluidine blue stain; 84-year-old woman. Section passes through optic nerve head at the left and foveola in the center.

upright and individually resolvable where pulled by detaching retina.[22,24] Even in attached specimens, outer segments (OSs) were frequently compacted. Although these factors can compromise SDD morphology and impair its recognition, histological sections were interpretable. Only a solid flocculent material that also appeared in attached specimens was called SDD. Other materials in the subretinal compartment, including isolated cells, oil droplets, pigment granules, and a fine proteinaceous substance, were distinguishable from SDD. Scattered or loosely packed SDD-like components or empty spaces between fascicles of RPE microvilli were not called SDD. Because it is possible that other SDD forms did not survive processing, our estimates of SDD thickness, coverage, and prevalence should be considered lower bounds. Accordingly, we did not adapt a spectral domain optical coherence tomography grading scale for SDD and SDD-associated outer retinal hyperreflective band deflections[1] to histological sections.

Within the sub-RPE compartment, a grayish-pink layer of nonuniform thickness was called BlinD (Figure 3, B and C arrowheads) and distinguished from a grayish-pink layer of uniform thickness (Figure 3C, arrows) thought to represent stacked lipoprotein particles on the inner surface of the Bruch membrane of many older eyes.[15,25,26] Other sub-RPE components included drusen, presumed Müller cells extending externally from the Henle fiber layer in neurosensory retina,[27] pigment-containing cells, and fluid.

Lesion prevalence was determined from thicknesses measured at sampling locations. Sampling locations were classified as SDD only, BlinD only, both SDD + BlinD, or neither lesion, and associations of these lesion with RPE status and BlamD thickness at the same eccentricity were computed. In the analysis of macular subregions, locations $\leq$0.6 mm from the foveal center on the section through the foveola were called fovea. Those on either side were nasal or temporal perifovea. In sections through superior perifovea, the percentage of RPE-Bruch membrane length covered by SDD (coverage) was computed.

Morphometric characteristics were compared between lesion groups using mixed statistical models and generalized estimating equations for continuous (e.g., BlamD thickness) and categorical (e.g., RPE pathology grade) variables, respectively, to account for data clustering (i.e., multiple sections from individual eyes and the fellow eyes). Calculation of lesion prevalence on a per donor basis included only one eye per donor.

Results

Study Eyes

Results are presented from 22 eyes of 20 white donors (14 women and 6 men; mean age, 83.1 ± 7.7 years) at early (n = 17) and advanced (n = 5) stages of non-neovascular AMD. Five of 9 donors with clinical histories were diagnosed with non-neovascular AMD

COLOR

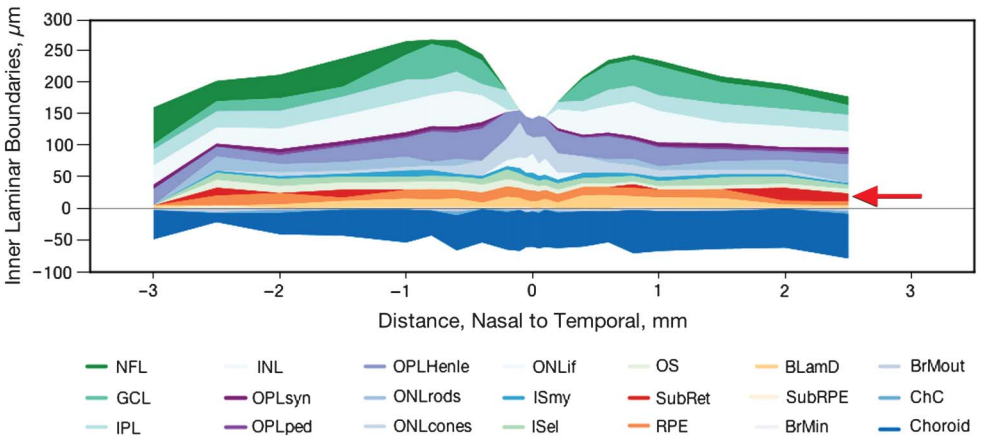

Fig. 2. Histologic layer thicknesses in non-neovascular AMD. Thicknesses of 21 chorioretinal layers in a 93-year-old male donor, measured from digital slides using a custom ImageJ plug-in. Subretinal drusenoid deposit foci in nasal and temporal perifovea are shown in red. BlamD is also prominent in this eye (yellow-orange; mean, 12.3 ± 7.8 μm; maximum, 24.9). BlinD is included in the sub-RPE space (cream colored). IS, inner segments; ONL, outer nuclear layer; OPL, outer plexiform layer; NFL, nerve fiber layer; INL, inner nuclear layer; GCL, ganglion cell layer; IPL, inner plexiform layer.

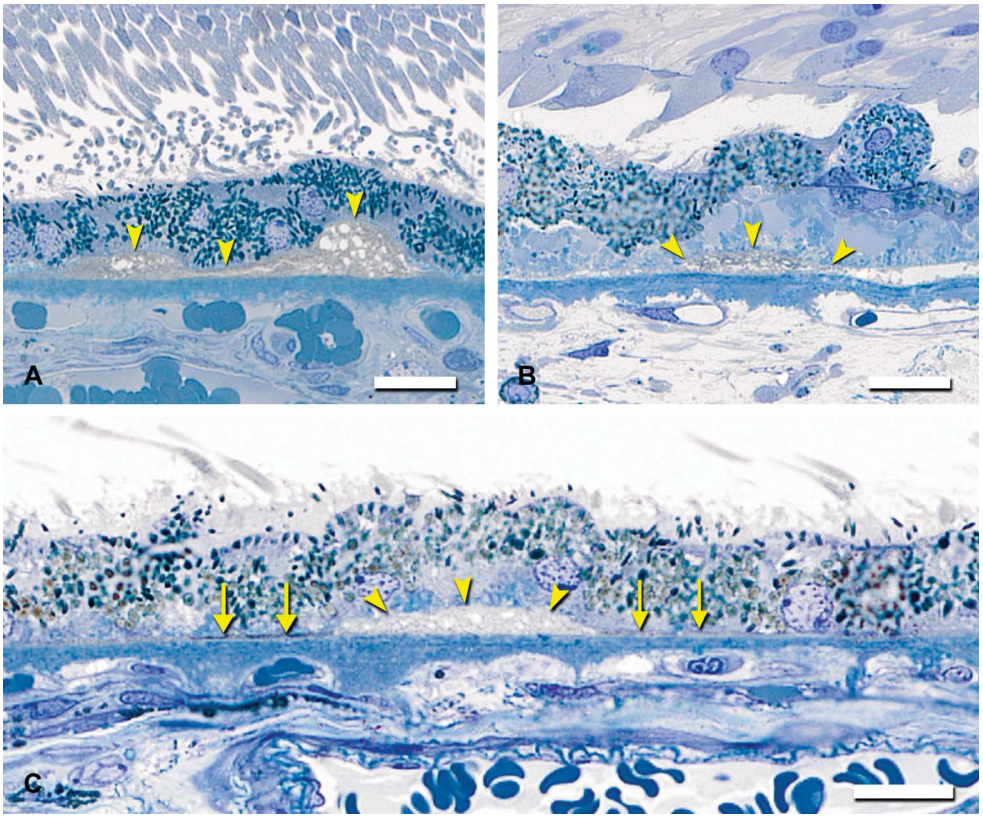

Fig. 3. Basal linear deposits in atrophic AMD eyes. A 0.8-μm-thick epoxy resin section, toluidine blue stain. Different eyes are shown. **A** and **B.** BlinD is grayish-pink material between the RPE basal lamina (yellow arrowheads) and the Bruch membrane, in drusenoid (**A**) and diffuse (**B**) forms. Eye in panel **B** has thick late basal laminar deposits; 88-year-old woman. Bars = 10 μm. **C.** A pocket of BlinD (yellow arrowheads) is flanked by a thin grayish-pink layer of uniform thickness (arrows, "Lipid Wall"[15,25,26]); 93-year-old man. Bar = 20 μm.

COLOR

2.1 months to 41.2 months before death. Others had clinically unremarkable maculas.

Subretinal Drusenoid Deposit Morphology

Subretinal drusenoid deposit was found as either isolated or confluent drusenoid mounds or dollops.[9] Figure 4A shows isolated SDD, which dominate in the valleys between conventional drusen. The middle formation in Figure 4A has an apical cap of medium staining and irregular oval inclusions ~1 μm in diameter, superficially resembling a condensate of OS-like material[28] but lacking internal structure resembling disks. Other nearby formations lacking this cap have internal septa. In this specimen with an attached retina, photoreceptor morphology is disturbed over all SDD formations, manifest as OS shortening (Figure 4A, Numbers 1 and 3) and OS loss with inner segment deflection and absence (Figure 4A, Number2). The largest SDD encroached on photoreceptors, apparent even in detached retinas, in which the border formed by OS tips was scalloped rather than straight (not shown), and the lesion itself was decapitate. Figure 4B shows the best-preserved example of perifoveal SDD in an eye where the retina is not only attached but also the photoreceptors are upright and closely apposed to the SDD internal surface. Here, confluent SDDs have septae of fasciculated apical processes (arrows).

Further details of sheet-like SDD morphology are shown in Figure 5. A formation in superior macula resembling reticular pseudodrusen ("ill-defined networks of broad interlacing ribbons"[29]) was apparent in ex vivo color photographs of one eye (Figure 5A) but not its fellow (Figure 5B) or others, presumably because of postmortem opacification of neurosensory retina. Apical processes in SDD-bearing eyes form regularly spaced bundles resembling uplifted arms along a scalloped RPE surface (Figure 5, C and D). Photoreceptor OS, mostly rods, seems associated with microvilli bundles, wrapping around SDD mounds to reach the RPE, as described.[7] Shortened photoreceptors abut SDD's inner surface, between bundles (Figure 5G). The narrowest SDD material visible by light microscopy in specimens with attached retinas or in sites where SDD was clearly delimited by microvilli bundles and associated OS tips is 8 μm to 17 μm, similar to the width of 1 to 2 RPE cells (Figure 5F). Whether this implies that some RPE do not touch photoreceptors is not certain, as SDD may contain tufts of apical processes visible in other sections. Perifoveal SDD was seen to be quite extensive. Median coverage of RPE by SDD in the superior perifovea of 20 eyes was 20.3% (section length 6.70 ± 0.70 mm). Five eyes had SDD coverage of ≥62.4%. In Figure 6, SDD overlies numerous partially

COLOR

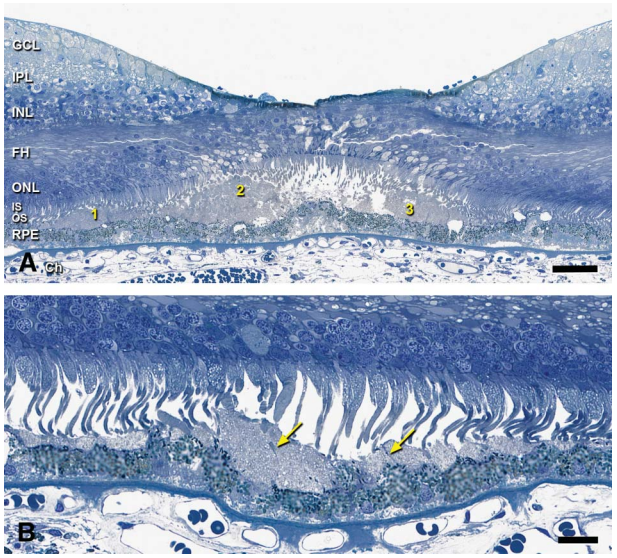

Fig. 4. Subretinal drusenoid deposit morphology. A 0.8-μm-thick epoxy resin section, toluidine blue stain; 80-year-old man. **A.** This foveal center has dysmorphic RPE, basal laminar deposits, basal mounds, and three discrete SDD formations. Formation 2 is a drusenoid dollop with an apical cap of medium staining, irregular oval inclusions ~1 μm in diameter, superficially resembling a condensate of OS-like material. Formations 1 and 3 lack this cap and have internal septa. Photoreceptor morphology is disturbed over all formations, manifest as OS shortening (1 and 3), and OS loss with inner segment deflection and absence (2). Bar = 50 μm. **B.** At 1.8 mm nasal to the foveola, individual SDD formats are dollop shaped and as small as a single RPE cell. Subretinal drusenoid deposit contains vesicular components, and septa are apparent (arrows). Outer segments of overlying photoreceptors are closely apposed to SDD internal surface where they may contribute to the septa. Bar = 20 μm. IS, inner segments; ONL, outer nuclear layer; INL, inner nuclear layer; GCL, ganglion cell layer; FH, Henle fiber layer; IPL, inner plexiform layer.

intact soft drusen containing neutral lipid pools and additionally lies within inter-druse valleys.

Subretinal drusenoid deposit fine structure is similar but not identical to the contents of soft drusen, BlinD, and basal mounds, the classically described sites of membranous debris[2] (also called lipoprotein-derived debris[30]). In Figure 5C, SDD is packed with membranous profiles. In Figure 5D, SDD comprise a dispersed phase of deeply stained particulate material within a flocculent continuous phase. In these eyes, different compositional textures seem to vary on an eye-by-eye basis, that is, SDD with particulate interiors are found throughout that section. These findings may be because of between-eye differences in preservation quality or more intriguingly, to a distinct taxonomy of SDD morphological phenotypes, like that described for conventional drusen.

Lesion Prevalence, Topography, Relationship to Other Age-Related Macular Degeneration Pathology

Median SDD thickness was 9.4 μm (range, 3.4–51.1 μm; Q1 = 6.2 μm; Q3 = 13.6 μm). Median BlinD thickness was 1.8 μm (range, 0.5–34.4 μm; Q1 = 1.1 μm; Q3 = 4.6 μm). Subretinal drusenoid deposit was significantly thicker than BlinD (*t*-test for unequal variances, $P < 0.0001$).

Annotated layer thicknesses obtained through systematic sampling of retinal regions were used to quantify SDD and BlinD prevalences, topography, and lesion associations with other aspects of AMD pathology. Of 20 non-neovascular AMD donors covered by 1,000 sampling locations, 17 (85.0%) had SDD and 18 (90%) had BlinD, at any location. Under a stricter criterion of at least 3 affected locations per eye, SDD was present in 14/20 (70.0%), and BlinD in 13/20 (65.0%) of AMD donors. Individuals varied considerably in lesion extent, from 1 to 25 affected locations per eye for SDD (mean, 9) and 1 to 22 for BlinD (mean, 7). Variability in SDD and BlinD extent was not correlated ($P = 0.23$).

A striking observation was the abundance of BlinD and paucity of SDD in the fovea and the abundance of SDD in the superior perifovea (Table 1). Of sampling locations with SDD only, 9.9% were in the fovea and 90.1% were in the perifovea, in the order superior (62.0%) >> nasal (17.5%) >temporal (10.5%; $P < 0.0001$ for difference among regions; inferior retina was not sectioned). Of sampling locations with BlinD only, 57.1% were in the fovea and 42.9% were in the perifovea with similar proportions (12.0–15.8%) in nasal, superior, and temporal subregions. Topographies were also assessed by calculating the percentage of sampling locations in each macular subregion, that is, normalizing about the region rather than by the lesion group (Figure 7). This analysis shows that 34.5% of the foveal locations had BlinD compared with only 4.0% to 15.0% of the perifoveal locations. Conversely, 12.9% to 21.4% of the perifoveal locations had SDD compared with only 7.7% of the foveal locations. Pooling locations with drusen with those containing only BlinD did not change this conclusion (data not shown). A second striking observation is that any one location tended to have either SDD (17.1% of total locations) or BlinD (13.3%) but not both (only 2.3%). Thus, even in regions of topographic overlap, SDD and BlinD tend not to appear on opposite aspects of the same RPE cells, as previously noted.[11] Finally, both pairs of fellow eyes had highly concordant findings of abundant SDD and minimal BlinD.

We examined other aspects of AMD pathology at sampling locations with SDD, BlinD, or neither lesion. Retinal pigment epithelium morphology ranged from unaffected to atrophic (absence of a pigmented layer, with or without BlamD, Table 1) in these non-neovascular AMD eyes. Retinal pigment epithelium morphology was worse in locations with either SDD

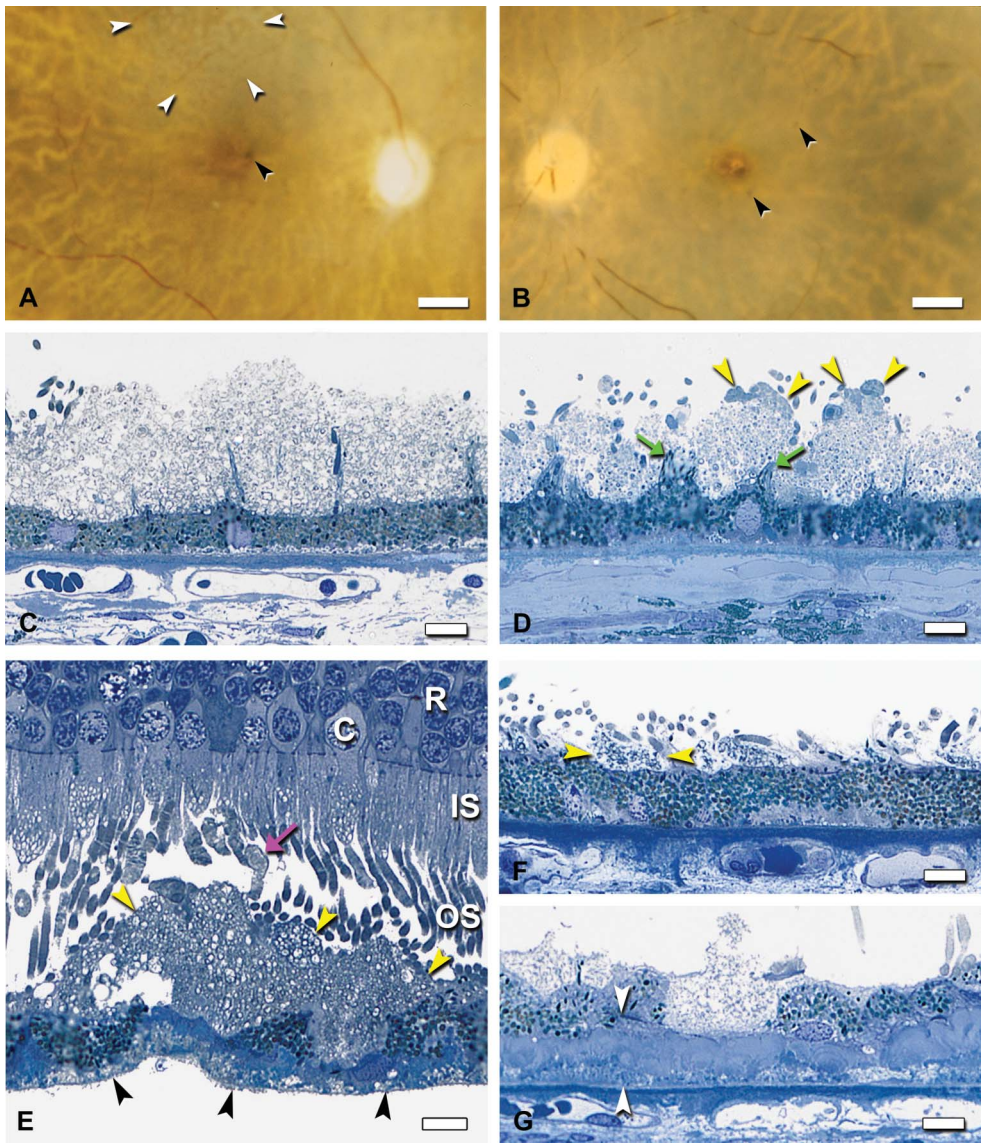

Fig. 5. Subretinal drusenoid deposit in the superior–temporal perifovea. Different eyes are shown. **A–D.** Postmortem macula and histopathology of fellow eyes with SDD (2000069R, 97-year-old woman). **A** and **B.** Reticular drusen superior to fovea (white arrowheads, **A**) and clumped pigment near fovea (black arrowheads, **A** and **B**). Film originals, epi-illumination and retro-illumination; bars = 1 mm. **C** and **D.** Subretinal drusenoid deposit is distinct from apical processes, which form regularly spaced bundles, like goalposts along a scalloped apical surface (arrows, **D**). Subretinal drusenoid deposits have a dispersed phase of particulate material within a flocculent continuous phase. Relative to **D**, SDD in panel **C** is thicker, has less particulate material, and lacks associated photoreceptor OSs and partial caps. Bars = 10 μm. **E.** Photoreceptors, mostly rods, overlying large SDD mound. Most OSs abut SDD in an unremarkable manner. Some OSs are bulbous, lightly stained, and lacking normal disk structure (arrow). Fringe on basolateral surface of detached RPE is BlinD (black arrowheads). C, cone nucleus; IS, inner segments; R, rod nucleus. Bar = 10 μm. **F.** The smallest SDDs were delimited by bundles of apical processes (arrowheads) and associated OS tips. They were similar in size to 1 to 2 RPE cells. **G.** An RPE cell is replaced by SDD. Arrowheads delimit thick basal laminar deposits. A 0.8-μm-thick sections, toluidine blue stain.

COLOR

or BlinD compared with locations with neither lesion ($P < 0.0001$). More locations with BlinD only were associated with atrophic RPE (14.0%) than with SDD only (0.6%; $P = 0.0036$). BlamD, considered as a marker of AMD progression,[3] was present at 76.8% of locations with SDD only and 81.5% of locations with BlinD only. BlamD was thicker (6.2 μm) at locations associated with BlinD than at locations associated with SDD only (4.2 μm; $P < 0.03$). Finally, we checked for vascular changes associated with SDD and BlinD. Choriocapillary ghosts are recognized readily by the absence of endothelial cells in an arch-like space delimited by intercapillary pillars.[31,32] Ghosts were present in similar proportions at locations with SDD + BlinD and with neither lesion (7.7 and 8.7%, respectively, Table 1). They were higher in areas with either lesion, especially sites with BlinD only (17.3%). We also examined the choroid external to these lesions for signs of vascular sclerosis[10] or other abnormalities and primarily noted overall choroidal thinning, loss of large vessels, and hyalinization of stroma throughout the macula.

Discussion

This is the largest series of eyes devoted to histologic characterization of SDD and the first study to compare thicknesses and topographies of AMD-specific lesions. We solidify previous observations from smaller series of AMD and non-AMD eyes[2,4,6,7,11,28] that SDD is an organized and stereotypical lesion that is readily

COLOR

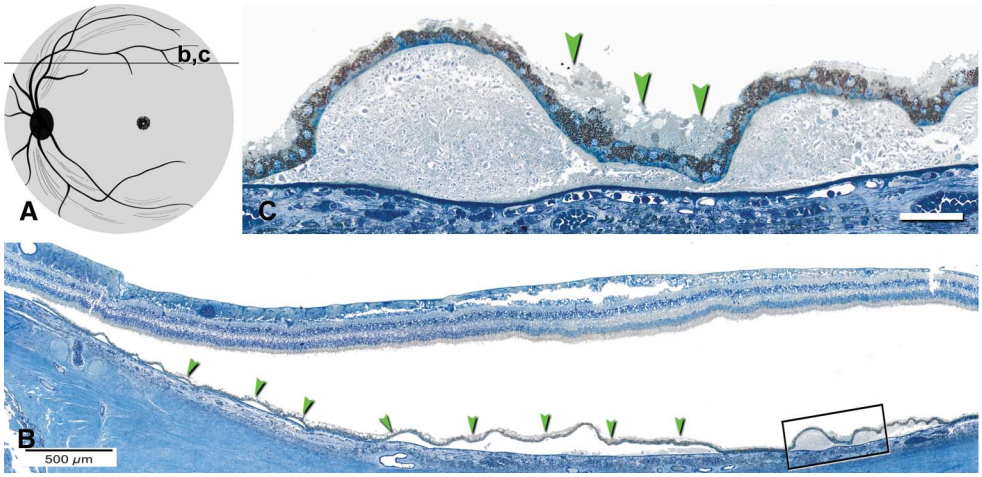

Fig. 6. Subretinal drusenoid deposits is abundant in superior perifovea. **A.** Schematic representation of a section 2,000 μm superior to the foveal center that is illustrated in panels **B** and **C. B.** Extensive SDD (arrowheads) overlying numerous partially intact soft drusen. Boxed area is shown in panel (**C**). **C.** Subretinal drusenoid deposit (arrowheads) lies between confluent large soft drusen that contain neutral lipid pools. **B** and **C.** A 0.8-μm-thick epoxy resin section, toluidine blue stain; 80-year-old man. Bar in panel **C**, 50 μm.

distinguishable from other subretinal components and from extracellular lesions in other compartments. Its association in attached retinas with deflected and shortened photoreceptors supports the idea that the lesions are in place during life and are not relocated by processing artifact.[28,33] Our principal new finding is SDD preferentially localizes to the perifovea, a location where there is a high density of rods, whereas BlinD is thickest in the fovea, where there is a high density of cones[21] (Figure 8). Results suggest that SDD and BlinD reflect differential aspects of rod and cone physiology, linking macular photoreceptor topography and AMD pathology.

Subretinal drusenoid deposit and BlinD are common in non-neovascular AMD, yet SDD has come to the fore only recently. Subretinal drusenoid deposit's first

Table 1. Subretinal Drusenoid Deposit and BlinD Morphometric and Histologic Associations at Sampling Locations

	Neither Lesion		SDD Only		BlinD Only		SDD + BlinD	
Macular subregion	n	%	n	%	n	%	n	%
Fovea	124	18.4	17	9.9	76	57.1	3	13.0
Nasal	93	13.8	30	17.5	16	12.0	1	4.4
Superior	355	52.8	106	62.0	20	15.0	19	82.6
Temporal	101	15.0	18	10.5	21	15.8	0	0.0
Perifovea (N + S + T)	549	81.6	154	90.1	57	42.9	20	87.0
All regions (F + N + S + T)	673	67.3	171	17.1	133	13.3	23	2.3
$P < 0.0001$ for fovea vs. nasal, superior, and temporal; fovea vs. perifovea								
RPE pathology grade	n	%	n	%	n	%	n	%
0, 1 (normal aging)	107	30.4	47	27.8	30	23.1	1	4.4
2 (very heterogeneous)	114	32.4	96	56.8	52	40.0	16	69.6
2A, 2B, 2L (reactive)	57	16.2	17	10.1	24	18.5	5	21.7
3 (intraretinal)	32	9.1	8	4.7	5	3.9	0	0.0
4, 5 (atrophic with and without BlamD)	42	11.9	1	0.6	19	14.6	1	4.4
$P < 0.0001$ for differences among lesion groups; $P = 0.0036$ for SDD only vs. BlinD only, Grades 4 and 5 vs. Grades 0 and 1								
BlamD thickness	n	μm	n	μm	n	μm	n	μm
	673	5.22 ± 6.05	171	4.22 ± 4.03	133	6.20 ± 5.52	23	4.75 ± 3.77
$P < 0.03$ for differences among lesion groups								
Choriocapillaris	n	%	n	%	n	%	n	%
No ghost	621	92.3	150	87.7	110	82.7	21	91.3
Ghost	52	7.7	21	12.3	23	17.3	2	8.7
$P < 0.0001$ for differences between neither and SDD only, BlinD only								

Number of sampling locations in 4 lesion groups in 22 eyes is 673, 171, 133, and 23 for macular subregions, BlamD, and choriocapillaris, and 352, 169, 133, and 23 for RPE. Retinal pigment epithelium pathology grades adapted from Vogt et al and Rudolf et al[22,23]: 0, uniform pigmentation and morphology; 1, nonuniform morphology and pigmentation; 2, very nonuniform morphology and pigmentation but still epithelioid; 2A, rounding and sloughing of individual cells from the underlying substrate (either the Bruch membrane or a layer of basal deposits); anterior migration of cells within the subretinal space; 2B, pigmented cellular fragments within basal laminar deposit; 2L, double layer of continuous RPE; 3, anterior migration through the external limiting membrane and into neurosensory retina; 4, loss of pigmented cells with persisting basal laminar deposits; 5, absence of pigmented cells and basal laminar deposit.

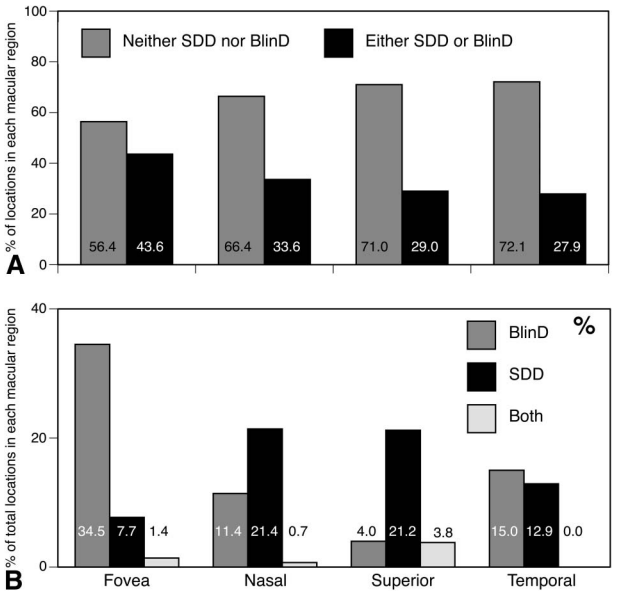

Fig. 7. Prevalence of SDD and BlinD. Percentages of sampling locations, pooled across 22 non-neovascular AMD eyes, have been normalized to number of sampling locations per macular subregion. **A.** Overall lesions are more prevalent in the fovea. **B.** Subretinal drusenoid deposit is more prominent than BlinD in nasal, superior, and temporal perifovea. BlinD is more prominent in the fovea. Few locations have both SDD and BlinD.

2 histologic descriptions were separated by 15 years and pertained to 2 different diseases.[2,28] The first 2 descriptions in AMD eyes were separated by 17 years.[2,4] Subretinal drusenoid deposit was not reported in histologic surveys of AMD eyes using paraffin[19,34,35] or cryosections,[36–38] likely because its optimal visualization requires osmium postfixation, semi- or ultrathin sections, and samples that include nonfoveal macula. Ultrastructural studies, including

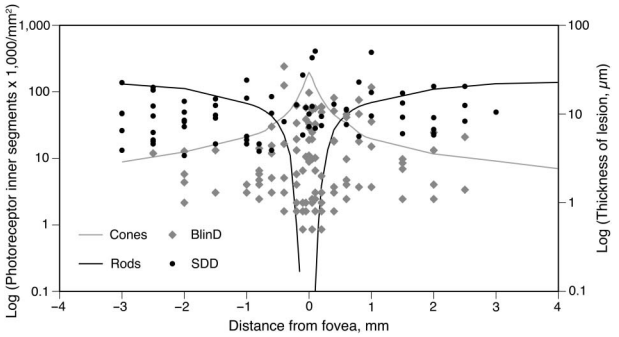

Fig. 8. Subretinal drusenoid deposit and BlinD thicknesses and photoreceptor topography. Lesion thicknesses in foveal sections of 20 non-neovascular AMD eyes and plotted for comparison with the spatial density (cells per square millimeter) of photoreceptor inner segments along the horizontal meridian in adult human retina.[21] In this log plot, zero densities and thicknesses are not shown. The photoreceptor mosaic is cone dominated at ≤0.5 mm eccentricity and rod dominated elsewhere. Both SDD and BlinD are found across the macula. However, SDD is thick and prevalent in rod-rich macular regions. BlinD is thin and prevalent in cone-rich macular regions.

our own, tended to concentrate on fovea[2,3,5,12,39,40] or did not specify sample location.[41] Finding SDD requires looking for it, and seeing it in enough attached specimens to enable informed interpretation of detached specimens, which, in turn, implies tissues obtained quickly after donor death. In this study, we used high-resolution sections of short postmortem (<3 hours) tissues postfixed to preserve neutral lipids in AMD's characteristic lesions. Finally, SDD's significance became apparent only when new clinical imaging technologies such as spectral domain optical coherence tomography enabled visualization of a widely distributed lesion with a distinctive morphology, topography, and independent risk levels for progression.[1,42,43]

A major question is whether SDD accounts for the clinical appearance of pseudodrusen described by different investigators using various high-resolution instruments. Several salient features of reticular pseudodrusen can be related to our current or past[7] histologic data: 1) Descriptions of interlacing yellow material or networks.[29,44] 2) High prevalence in AMD eyes, especially geographic atrophy,[45] with prevalence estimates varying widely with detection method[45] and patient population (Table 2). 3) Bilateral symmetry.[42,55] 4) Abundance in the superior and superior–temporal macula, with more outside the macula superiorly[1,10,29,51,56,57] and little[10,51] in the central macula. 5) Dynamism over time, with expansion into superior retina[10,11] and continuous focal enlargement and anterior migration into the retina.[58] It would be remarkable with this level of correspondence if SDDs were not the histologic correlate of reticular pseudodrusen, as it would imply that another feature of this magnitude in the same region remains to be detected clinically. Furthermore, the varying clinical appearances, ranging from dots to ribbons, raise the possibility of multiple SDD subtypes or stages of progression or both, with distinctive ultrastructural correlates and compositions. The name reticular pseudodrusen appears inaccurate for this lesion, which is neither universally reticular (network), pseudo (false), nor drusen (sub-RPE).

A comprehensive theory of AMD extracellular lesion formation would ideally account for both SDD and sub-RPE drusen/BlinD. An existing model for BlinD involving its largest component, cholesterol-rich lipoproteins containing apolipoproteins B and E,[30,59] is summarized as Steps 1 to 4 in Figure 9. We hypothesize that the RPE is a polarized and bidirectional secretor of lipoproteins which serve photoreceptor and RPE physiology driven by OS membrane lipid composition and that these lipoproteins participate in lesion formation in two compartments, as follows.

Table 2. Clinical Studies Reporting Reticular Drusen/SDD Prevalence (Chronological Order)

Reference	Patient Population*	Imaging Modality	% Affected
10	Newly presenting AMD cases	Various	13.0
46	Non-AMD fellow eye	Red free	3.0
47	AMD		20.0
48	Early AMD; non-neovascular AMD	FAF-SW	8.4
48	CNV	FAF-SW	36.0
49	Exudative AMD		24.0
50	Population based; >80 years	Color fundus photos†	30.0
51	Population based; 75–86 years	Color fundus photos	2.4
42	Late AMD	SD OCT	33.0
45	Geographic atrophy	FAF-SW	55.7
45	Geographic atrophy	IR reflectance	59.1
52	Geographic atrophy	Various	91.0
53	Geographic atrophy	FAF-SW	92.3
54	Atrophic AMD	FAF-SW, FAF-NIR	29.0

*As described by authors; FAF-SW, fundus autofluorescence, short wavelength (488 nm excitation); FAF-NIR, fundus autofluorescence, near infrared (830 nm excitation).
†Combined with indistinct drusen.
SD OCT, spectral domain optical coherence tomography.

Strong circumstantial evidence suggests that one or more high-density lipoprotein (HDL) classes subserve intraretinal lipid transport, including a rapid distribution of lipoprotein-delivered UC from the choroid into neurosensory retina.[64] High-density lipoproteins are multifunctional multimolecular assemblies consisting of an esterified cholesterol–rich core solubilized by surface components of apolipoproteins and phospholipids. Plasma HDL, 7 to 11 nm in diameter, is notable for multiple classes defined by different isolation techniques and by extensive extracellular remodeling via enzymes and transfer proteins. These include lecithin acyl cholesterol transferase (LCAT), cholesterol ester transfer protein (CETP), phospholipid transfer protein (PLTP), and hepatic lipase (LIPC).[66,67] In reverse cholesterol transport, plasma HDL receives UC from cellular membranes throughout the body via ATP-binding cassette A-I (ABCA-1) for transport to liver, where scavenger receptors (SRB-I, II) mediate selective esterified cholesterol uptake. High-density lipoprotein carries >100 proteins, including complement factors and coagulation factors. Fewer than half subserve lipid metabolism.[68] Brain cerebrospinal fluid, embryologically equivalent to the subretinal space, also harbors HDL-like lipoproteins containing apoE. These serve the rich lipid traffic between astrocytes and neurons, subject to remodeling via intracerebrally expressed LCAT, CETP, and PLTP.[69–71] Of relevance to SDD, variants in CETP and LIPC genes modify AMD risk independent of plasma HDL levels.[72–74] ApoE, CETP, LIPC, LCAT, and SRB-II immunoreactivity, along with PLTP activity, localize to interphotoreceptor matrix.[64,75] ApoE is secreted by RPE and Müller cells, appearing in aspirates from rhegmatogenous retinal detachments.[76–80] Subretinal drusenoid deposit contains complement cascade components and regulators.[7,81] Thus, numerous molecules with well-known HDL associations are present in the subretinal space.

Rod OS disks pinch off from the plasma membrane near the inner segment. They become internal membranes, which unlike plasma membranes are low in UC content (10% vs. 30–35%).[82,83] In transit from OS base to tip,[62] disks reduce UC and increase the fatty acid docosahexaenoate (DHA) within phospholipids (Step 5, Figure 9). These changes enable the conformational flexibility of rhodopsin required by single-photon sensitivity. Outer segment–derived DHA stored in RPE after disk shedding and phagocytosis are recycled back to inner segments[63,84] by an as-yet unspecified mechanism. High-density lipoprotein particles cycling between RPE and photoreceptors, proposed for intraretinal lipid transfer to inner segments,[64] could move both UC from, and DHA to, OS disks progressing toward the RPE. In contrast (Step 6, Figure 9), cone OS disks are comb-like projections of plasma membrane and are believed to maintain high UC content along their length (unpublished observations; personal communication, R. Mullins, PhD, May 2012).[62] Cone OS UC enters RPE via disk shedding and lysosomal uptake. This UC is released for intracellular transfer, esterification, and assembly into basolaterally secreted apoB,E-containing lipoproteins, especially under cone-dominant fovea, where they form the basis of BlinD (Steps 3 and 4, Figure 9). Using perturbation of cholesterol homeostasis and lipid transfer as unifying mechanisms, it may be possible to explain the formation of SDD in areas enriched with rods and BlinD under the cone-dominant fovea, with

COLOR

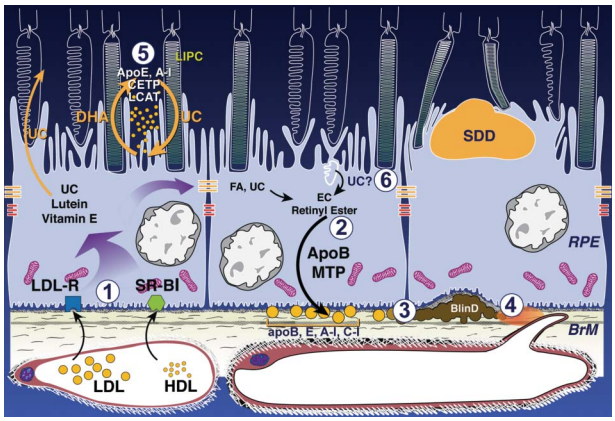

Fig. 9. Biogenesis of sub-RPE and subretinal AMD lesions: model normal at left center and AMD at right. Described in Zweifel et al and Curcio et al.[1,59] BlinD, current 1) plasma lipoproteins delivering lipophilic nutrients enter RPE.[60] 2) ApoB,E lipoproteins secreted basolaterally by RPE[61] (gold circles) are assembled from multiple lipid sources. Fatty acids are dominated by linoleate, implicating internalized plasma lipoproteins as a major source. Unesterified cholesterol from all sources is esterified to esterified cholesterol. 3) Lipoproteins are retained by interacting with BrM extracellular matrix and accumulate throughout adulthood, creating a lipid wall on BrM's inner surface. 4) Reactive oxygen species from neighboring mitochondria promote appearance of proinflammatory and toxic moieties. Lipoproteins fuse and form lipid pools and UC-rich liposomes within BlinD/soft drusen, rendering them biomechanically unstable. Subretinal drusenoid deposit, new 5) disks in rod OS lose UC and gain docosahexaenoate in transit from OS base to tip[62] (shown as loss of white). Outer segment–derived DHA stored as triglycerides in RPE after phagocytosis return to OS.[63] High-density lipoprotein particles cycling between RPE and photoreceptors[64] could handle both transfers as part of a vectorial lipid flow retainable within interphotoreceptor matrix as UC-containing SDD, especially under rod-rich perifovea. BlinD, new 6) cone OS maintain high UC content along their length because their disks are comb-like projections of plasma membrane.[62] Cone OS UC enters RPE via disk shedding, lysosomal uptake, and acid lipase activity.[65] Unesterified cholesterol is released for intracellular transfer, esterification, and assembly into basolaterally secreted lipoproteins, especially under cone-rich fovea.

downstream negative consequences, such as inflammation, in both compartments.

Strengths of this work include short postmortem donor eyes, time-of-study histopathologic AMD ascertainment as opposed to clinical histories obtained at variable premortem intervals, a tissue preparation technique designed to improve neutral lipid preservation, a quantized RPE grading scale, and a retina-centered coordinate system and systematic sampling that together facilitated statistical analysis across eyes. Limitations include postmortem retinal detachment, absence of extensive serial section reconstruction, limited clinical histories that did not include imaging or genotype, and the subjective nature of histologic judgments.

Reflecting remarkable compartmentalization of photoreceptor, RPE, and the Bruch membrane functions, AMD's lesions reflect different biologic pathways deployed with micrometer precision in the vertical axis. BlinD and soft drusen are external to RPE basal lamina, and SDD is subretinal and likely reflect activity along distinct pathways within polarized RPE.[85] The fovea is the region with the highest packing density of cones, and cone damage and destruction is an important consequence of late AMD. This is the first study to show that rods may play an important pathophysiologic stimulus for the development of AMD because of the formation of SDD. As a component of early AMD, SDD is a recognized risk factor for the development of both geographic atrophy and choroidal neovascularization.

Key words: age-related macular degeneration, basal linear deposit, cholesterol, fovea, histopathology, lipoproteins, macula, photoreceptors, reticular drusen, subretinal drusenoid deposit.

References

1. Zweifel SA, Spaide RF, Curcio CA, et al. Reticular pseudodrusen are subretinal drusenoid deposits. Ophthalmology 2010; 117:303–312. e.1.
2. Sarks JP, Sarks SH, Killingsworth MC. Evolution of geographic atrophy of the retinal pigment epithelium. Eye 1988; 2:552–577.
3. Sarks S, Cherepanoff S, Killingsworth M, Sarks J. Relationship of basal laminar deposit and membranous debris to the clinical presentation of early age-related macular degeneration. Invest Ophthalmol Vis Sci 2007;48:968–977.
4. Curcio CA, Presley JB, Medeiros NE, et al. Esterified and unesterified cholesterol in drusen and basal deposits of eyes with age-related maculopathy. Exp Eye Res 2005;81:731–741.
5. Rudolf M, Clark ME, Chimento M, et al. Prevalence and morphology of druse types in the macula and periphery of eyes with age-related maculopathy. Invest Ophthalmol Vis Sci 2008;49:1200–1209.
6. Wolkow N, Song Y, Wu TD, et al. Aceruloplasminemia: retinal histopathologic manifestations and iron-mediated melanosome degradation. Arch Ophthalmol 2011;129:1466–1474.
7. Rudolf M, Malek G, Messinger JD, et al. Sub-retinal drusenoid deposits in human retina: organization and composition. Exp Eye Res 2008;87:402–408.
8. Mimoun G, Soubrane G, Coscas G. Macular drusen [in French]. J Fr Ophtalmol 1990;13:511–530.
9. Spaide RF, Curcio CA. Drusen characterization with multimodal imaging. Retina 2010;30:1441–1454.
10. Arnold JJ, Sarks SH, Killingsworth MC, Sarks JP. Reticular pseudodrusen. A risk factor in age-related maculopathy. Retina 1995;15:183–191.
11. Sarks J, Arnold J, Ho IV, et al. Evolution of reticular pseudodrusen. Br J Ophthalmol 2011;95:979–985.
12. Curcio CA, Millican CL. Basal linear deposit and large drusen are specific for early age-related maculopathy. Arch Ophthalmol 1999;117:329–339.
13. Curcio CA, Messinger JD, Mitra AM, et al. Human chorioretinal layer thicknesses measured using macula-wide high resolution histological sections. Invest Ophthalmol Vis Sci 2011; 52:3943–3954.
14. Curcio CA, Medeiros NE, Millican CL. The Alabama age-related macular degeneration grading system for donor eyes. Invest Ophthalmol Vis Sci 1998;39:1085–1096.

15. Curcio CA, Millican CL, Bailey T, Kruth HS. Accumulation of cholesterol with age in human Bruch's membrane. Invest Ophthalmol Vis Sci 2001;42:265–274.
16. Guyton JR, Klemp KF. Ultrastructural discrimination of lipid droplets and vesicles in atherosclerosis: value of osmium-thiocarbohydrazide-osmium and tannic acid-paraphenylenediamine techniques. J Histochem Cytochem 1988;36:1319–1328.
17. Curcio CA, Messinger JD, Sloan KR, Medeiros NE, and McGwin G, Jr. Biometrics and impact of basal linear deposit in non-neovascular age-related macular degeneration. In preparation.
18. Spraul CW, Lang GE, Grossniklaus HE. Morphometric analysis of the choroid, Bruch's membrane, and retinal pigment epithelium in eyes with age-related macular degeneration. Invest Ophthalmol Vis Sci 1996;37:2724–2735.
19. Sarks SH. Ageing and degeneration in the macular region: a clinico-pathological study. Br J Ophthalmol 1976;60:324–341.
20. Curcio CA, Allen KA. Topography of ganglion cells in human retina. J Comp Neurol 1990;300:5–25.
21. Curcio CA, Sloan KR, Kalina RE, Hendrickson AE. Human photoreceptor topography. J Comp Neurol 1990;292:497–523.
22. Vogt SD, Curcio CA, Wang L, et al. Retinal pigment epithelial expression of complement regulator CD46 is altered early in the course of geographic atrophy. Exp Eye Res 2011;93:413–423.
23. Rudolf M, Vogt SD, Curcio CA, et al. Histological basis of variations in retinal pigment epithelium autofluorescence in eyes with geographic atrophy. Ophthalmology 2012; Accepted September 19, 2012.
24. Marmorstein LY, McLaughlin PJ, Peachey NS, et al. Formation and progression of sub-retinal pigment epithelium deposits in Efemp1 mutation knock-in mice: a model for the early pathogenic course of macular degeneration. Hum Mol Genet 2007; 16:2423–2432.
25. Ruberti JW, Curcio CA, Millican CL, et al. Quick-freeze/deep-etch visualization of age-related lipid accumulation in Bruch's membrane. Invest Ophthalmol Vis Sci 2003;44:1753–1759.
26. Huang J-D, Presley JB, Chimento MF, et al. Age-related changes in human macular Bruch's membrane as seen by quick-freeze/deep-etch. Exp Eye Res 2007;85:202–218.
27. Kuntz CA, Jacobson SG, Cideciyan AV, et al. Sub-retinal pigment epithelial deposits in a dominant late-onset retinal degeneration. Invest Ophthalmol Vis Sci 1996;37:1772–1782.
28. Arnold JJ, Sarks JP, Killingsworth MC, et al. Adult vitelliform macular degeneration: a clinicopathological study. Eye 2003; 17:717–726.
29. Klein R, Davis MD, Magli YL, et al. The Wisconsin age-related maculopathy grading system. Ophthalmology 1991; 98:1128–1134.
30. Curcio CA, Johnson M, Huang J-D, Rudolf M. Aging, age-related macular degeneration, and the response-to-retention of apolipoprotein B-containing lipoproteins. Prog Retin Eye Res 2009;28:393–422.
31. McLeod DS, Lutty GA. High-resolution histologic analysis of the human choroidal vasculature. Invest Ophthalmol Vis Sci 1994;35:3799–3811.
32. Mullins RF, Johnson MN, Faidley EA, et al. Choriocapillaris vascular dropout related to density of drusen in human eyes with early age-related macular degeneration. Invest Ophthalmol Vis Sci 2011;52:1606–1612.
33. Johnson PT, Lewis GP, Talaga KC, et al. Drusen-associated degeneration in the retina. Invest Ophthalmol Vis Sci 2003;44: 4481–4488.
34. van der Schaft TL, Mooy CM, de Bruijn WC, et al. Histologic features of the early stages of age-related macular degeneration. Ophthalmology 1992;99:278–286.
35. Green WR, Enger C. Age-related macular degeneration histopathologic studies: the 1992 Lorenz E. Zimmerman Lecture. Ophthalmology 1993;100:1519–1535.
36. Kamei M, Hollyfield JG. TIMP-3 in Bruch's membrane: changes during aging and in age-related macular degeneration. Invest Ophthalmol Vis Sci 1999;40:2367–2375.
37. Malek G, Li C-M, Guidry C, et al. Apolipoprotein B in cholesterol-containing drusen and basal deposits in eyes with age-related maculopathy. Am J Pathol 2003;162:413–425.
38. Luibl V, Isas JM, Kayed R, et al. Drusen deposits associated with aging and age-related macular degeneration contain nonfibrillar amyloid oligomers. J Clin Invest 2006;116:378–385.
39. Sarks SH, van Driel D, Maxwell L, Killingsworth M. Softening of drusen and subretinal neovascularization. Trans Ophthalmol Soc U K 1980;100:414–422.
40. Curcio CA, Presley JB, Millican CL, Medeiros NE. Basal deposits and drusen in eyes with age-related maculopathy: evidence for solid lipid particles. Exp Eye Res 2005;80:761–775.
41. Hageman GS, Mullins RF. Molecular composition of drusen as related to substructural phenotype. Mol Vis 1999;5:28–37.
42. Zweifel SA, Imamura Y, Spaide TC, et al. Prevalence and significance of subretinal drusenoid deposits (reticular pseudodrusen) in age-related macular degeneration. Ophthalmology 2010;117:1775–1781.
43. Helb HM, Charbel Issa P, Fleckenstein M, et al. Clinical evaluation of simultaneous confocal scanning laser ophthalmoscopy imaging combined with high-resolution, spectral-domain optical coherence tomography. Acta Ophthalmol 2010;88:842–849.
44. Sohrab MA, Smith RT, Salehi-Had H, et al. Image registration and multimodal imaging of reticular pseudodrusen. Invest Ophthalmol Vis Sci 2011;52:5743–5748.
45. Schmitz-Valckenberg S, Alten F, Steinberg JS, et al. Reticular drusen associated with geographic atrophy in age-related macular degeneration. Invest Ophthalmol Vis Sci 2011;52:5009–5015.
46. Prenner JL, Rosenblatt BJ, Tolentino MJ, et al. Risk factors for choroidal neovascularization and vision loss in the fellow eye study of CNVPT. Retina 2003;23:307–314.
47. Einbock W, Moessner A, Schnurrbusch UE, et al. Changes in fundus autofluorescence in patients with age-related maculopathy. Correlation to visual function: a prospective study. Graefes Arch Clin Exp Ophthalmol 2005;243:300–305.
48. Smith RT, Chan JK, Busuoic M, et al. Autofluorescence characteristics of early, atrophic, and high-risk fellow eyes in age-related macular degeneration. Invest Ophthalmol Vis Sci 2006; 47:5495–5504.
49. Cohen SY, Dubois L, Tadayoni R, et al. Prevalence of reticular pseudodrusen in age-related macular degeneration with newly diagnosed choroidal neovascularisation. Br J Ophthalmol 2007;91:354–359.
50. Wang JJ, Rochtchina E, Lee AJ, et al. Ten-year incidence and progression of age-related maculopathy: the blue Mountains Eye Study. Ophthalmology 2007;114:92–98.
51. Klein R, Meuer SM, Knudtson MD, et al. The epidemiology of retinal reticular drusen. Am J Ophthalmol 2007;145:317–326.
52. Smith RT, Merriam JE, Sohrab MA, et al. Complement factor H 402H variant and reticular macular disease. Arch Ophthalmol 2011;129:1061–1066.
53. Smailhodzic D, Fleckenstein M, Theelen T, et al. Central areolar choroidal dystrophy (CACD) and age-related macular degeneration (AMD): differentiating characteristics in multimodal imaging. Invest Ophthalmol Vis Sci 2011;52:8908–8918.

54. Forte R, Querques G, Querques L, et al. Multimodal imaging of dry age-related macular degeneration. Acta Ophthalmol 2012;90:e281–e287.
55. Wang JJ, Mitchell P, Smith W, Cumming RG. Bilateral involvement by age-related maculopathy lesions in a population. Br J Ophthalmol 1998;82:743–747.
56. Smith RT, Sohrab MA, Busuioc M, Barile G. Reticular macular disease. Am J Ophthalmol 2009;148:733–743. e2.
57. Schmitz-Valckenberg S, Steinberg JS, Fleckenstein M, et al. Combined confocal scanning laser ophthalmoscopy and spectral-domain optical coherence tomography imaging of reticular drusen associated with age-related macular degeneration. Ophthalmology 2010;117:1169–1176.
58. Querques G, Poitrine FC, Coscas F, et al. Analysis of progression of reticular pseudodrusen by spectral domain optical coherence tomography. Invest Ophthalmol Vis Sci 2012;53: 1264–1270.
59. Curcio CA, Johnson M, Rudolf M, Huang J-D. The oil spill in ageing Bruch's membrane. Br J Ophthalmol 2011;95:1638–1645.
60. Tserentsoodol N, Sztein J, Campos M, et al. Uptake of cholesterol by the retina occurs primarily via a low density lipoprotein receptor-mediated process. Mol Vis 2006;12:1306–1318.
61. Johnson LV, Forest DL, Banna CD, et al. Cell culture model that mimics drusen formation and triggers complement activation associated with age-related macular degeneration. Proc Natl Acad Sci U S A 2011;108:18277–18282.
62. Albert AD, Boesze-Battaglia K. The role of cholesterol in rod outer segment membranes. Prog Lipid Res 2005;44:99–124.
63. Rodriguez de Turco EB, Parkins N, Ershov AV, Bazan NG. Selective retinal pigment epithelial cell lipid metabolism and remodeling conserves photoreceptor docosahexaenoic acid following phagocytosis. J Neurosci Res 1999;57:479–486.
64. Tserentsoodol N, Gordiyenko NV, Pascual I, et al. Intraretinal lipid transport is dependent on high density lipoprotein-like particles and class B scavenger receptors. Mol Vis 2006;12: 1319–1333.
65. Elner VM. Retinal pigment epithelial acid lipase activity and lipoprotein receptors: effects of dietary omega-3 fatty acids. Trans Am Ophthalmol Soc 2002;100:301–338.
66. Barter PJ. Hugh Sinclair lecture: the regulation and remodelling of HDL by plasma factors. Atheroscler Suppl 2002;3: 39–47.
67. Asztalos BF, Tani M, Schaefer EJ. Metabolic and functional relevance of HDL subspecies. Curr Opin Lipidol 2011;22:176–185.
68. Vaisar T, Pennathur S, Green PS, et al. Shotgun proteomics implicates protease inhibition and complement activation in the antiinflammatory properties of HDL. J Clin Invest 2007;117: 746–756.
69. Yu CJ, Youmans KL, LaDu MJ. Proposed mechanism for lipoprotein remodelling in the brain. Biochim Biophys Acta 2010;1801:819–823.
70. Hayashi H. Lipid metabolism and glial lipoproteins in the central nervous system. Biol Pharm Bull 2011;34:453–461.
71. Cramer PE, Cirrito JR, Wesson DW, et al. ApoE-directed therapeutics rapidly clear beta-amyloid and reverse deficits in AD mouse models. Science 2012;335:1503–1506.
72. Chen W, Stambolian D, Edwards AO, et al. Genetic variants near TIMP3 and high-density lipoprotein-associated loci influence susceptibility to age-related macular degeneration. Proc Natl Acad Sci U S A 2010;107:7401–7406.
73. Neale BM, Fagerness J, Reynolds R, et al. Genome-wide association study of advanced age-related macular degeneration identifies a role of the hepatic lipase gene (LIPC). Proc Natl Acad Sci U S A 2010;107:7395–7400.
74. Yu Y, Reynolds R, Fagerness J, et al. Association of variants in the LIPC and ABCA1 genes with intermediate and large drusen and advanced age-related macular degeneration. Invest Ophthalmol Vis Sci 2011;52:4663–4670.
75. Dudley PA, Anderson RE. Phospholipid transfer protein from bovine retina with high activity towards retinal rod disc membranes. FEBS Lett 1978;95:57–60.
76. Shanmugaratnam J, Berg E, Kimerer L, et al. Retinal Muller glia secrete apolipoproteins E and J which are efficiently assembled into lipoprotein particles. Mol Brain Res 1997;50: 113–120.
77. Schneeberger SA, Iwahashi CK, Hjelmeland LM, et al. Apolipoprotein E in the subretinal fluid of rhegmatogenous and exudative retinal detachments. Retina 1997;17:38–43.
78. Wong P, Pfeffer BA, Bernstein SL, et al. Clusterin protein diversity in the primate eye. Mol Vis 2000;6:184–191.
79. Anderson DH, Ozaki S, Nealon M, et al. Local cellular sources of apolipoprotein E in the human retina and retinal pigmented epithelium: implications for the process of drusen formation. Am J Ophthalmol 2001;131:767–781.
80. Ishida BY, Bailey KR, Duncan KG, et al. Regulated expression of apolipoprotein E by human retinal pigment epithelial cells. J Lipid Res 2004;45:263–271.
81. Ebrahimi KB, Wang L, Tagami M, et al. Oxidized low density lipoprotein-induced injury in RPE cells alters expression of the transmembrane complement regulatory factors CD46 and CD59 through exosomal and apoptotic bleb release. Invest Ophthalmol Vis Sci 53. E-Abstract 1650.
82. Dowhan W, Bogdanov M. Functional roles of lipids in membranes. In: Vance DE, Vance JE, eds. Biochemistry of Lipids, Lipoproteins and Membranes. Amsterdam, the Netherlands: Elsevier; 2002:1–35.
83. Boesze-Battaglia K, Fliesler SJ, Albert AD. Relationship of cholesterol content to spatial distribution and age of disk membranes in retinal rod outer segments. J Biol Chem 1990;265: 18867–18870.
84. Bazan NG, Gordon WC, Rodriguez de Turco EB. Docosahexaenoic acid uptake and metabolism in photoreceptors: retinal conservation by an efficient retinal pigment epithelial cell-mediated recycling process. Adv Exp Med Biol 1992;318: 295–306.
85. Curcio CA. Complementing apolipoprotein secretion by retinal pigment epithelium. Proc Natl Acad Sci U S A 2011;108: 18569–18570.